Comparison of rainfall profiles in the West African monsoon as depicted by TRMM PR and LMDZ climate model

Samo Diatta, Frédéric Hourdin, Amadou T. Gaye, Nicolas Viltard

Comparison of Rainfall Profiles in the West African Monsoon as Depicted by TRMM PR and the LMDZ Climate Model

SAMO DIATTA

Laboratoire de Physique de l'Atmosphere et de l'Ocean (LPAOSF), ESP/UCAD, Dakar, Senegal

FRÉDÉRIC HOURDIN

Laboratoire de Météorologie Dynamique, IPSL, Paris, France

AMADOU THIERNO GAYE

Laboratoire de Physique de l'Atmosphere et de l'Ocean (LPAOSF), ESP/UCAD, Dakar, Senegal

NICOLAS VILTARD

Laboratoire Atmospheres, Milieux, Observations Spatiales, IPSL, Paris, France

(Manuscript received 10 June 2009, in final form 4 November 2009)

ABSTRACT

Vertical rainfall profiles obtained with TRMM-PR 2A25 standard products are compared with rain profiles deduced from the Laboratoire de Météorologie Dynamique second generation global climate model (LMDZ, the Z stands for zoom capability) with two parameterization schemes: Emanuel's and Tiedke's. This paper focuses on the low layers of the atmosphere over West Africa during the monsoon [June–September (JJAS)]. The precipitation decrease above 4 km is systematically not represented in rainfall profiles generated by Emanuel's parameterization scheme. However, Emanuel's scheme shows a decrease similar to the observation from 4 km down to the surface, especially in the Sahel (proper depth of the layer dominated by reevaporation). As for Tiedtke's scheme, it best describes the downward increase in the upper levels of the atmosphere, whereas the downward decrease in the lower levels begins too low when compared to the observations.

Tiedtke's parameterization shows an overestimation of liquid water production over the ocean and over the Guinean region and a slightly too strong reevaporation in the Sahara and Sahel. The zonal distribution of vertical rain profiles is then biased with this model scheme compared to the 2A25-PR product. On the other hand, although Emanuel's scheme detects too much reevaporation over the Sahara and underestimates liquid water production over the ocean compared to PR observation, it shows a good meridional distribution of these parameters. This is especially true in the Sahel where Emanuel's scheme gives the best representation of reevaporation.

1. Introduction

Understanding precipitation systems and evaluating their contribution to the water cycle in West Africa is an important research issue. Rainfall over this region is controlled by the low levels of advection of moisture from the Gulf of Guinea. This advected moisture flow is the signature of the African monsoon that drives the north–south rain gradient between the coast and the Sahara. This moisture gradient also leads to specific water vapor profiles and surface–atmosphere exchanges as we move from the coast to the north. This induces a regional modulation of the rain reevaporation; wherever this reevaporation occurs, it induces a mesoscale downdraft driven by the adiabatic cooling from thermal exchanges (Zipser 1969; Leary and Houze 1979). This adiabatic cooling cancels at least partially the deep convective heating in regions of large-scale ascent (Bister

Corresponding author address: Samo Diatta, Laboratoire Physique de l'Atmosphere et de l'Ocean, Ecole Superieure Polytechnique, University Cheikh Anta Diop, P.O. Box 5085, Dakar Fann, Dakar, Senegal.
E-mail: samo.diatta@ucad.edu.sn

DOI: 10.1175/2009MWR3092.1

and Emanuel 1997). Additionally, the reevaporation of rainfall profiles is also responsible for the generation of cold pools of air or wakes, involved in the self-organization and propagation of the squall lines in West Africa.

Many efforts have been made to improve representation of convective rainfall in climate models since it remains a critical issue for the simulation of the current climate (Houghton et al. 2001). In particular, precipitating downdraft and reevaporation processes mentioned above were shown to be a key issue for the representation of the mean tropical climate (Hourdin et al. 2006; Braconnot et al. 2007) and its variability (Lin et al. 2006) in coupled ocean–atmosphere models. As storms propagate from initiation (genesis) to decay, they leave behind them footprints of condensation rate and evaporation rate at various levels of the troposphere. These features have an important impact on the circulation in tropics (e.g., Mapes and Houze 1993).

One way to understand dynamics and thermodynamics of these processes and their associated microphysics is to identify local variations of the vertical structure of precipitation systems (e.g., Geerts and Dejene 2005; Schumacher and Houze 2006; Houze 1981; Zipser and Lutz 1994) as measured since January 1998 by the Tropical Rainfall Measuring Mission (TRMM) Precipitation Radar (PR). Appropriate computation of statistics for vertical profiles of precipitation will help to infer some of the regional and seasonal characteristics of the reevaporation processes in the lower layers of the atmosphere.

The present study aims to characterize and compare the vertical profiles of precipitations obtained respectively with the TRMM PR radar and two different parameterizations schemes used in the Laboratoire de Météorologie Dynamique second generation global climate model (LMDZ, the Z stands for zoom capability). This study focuses mostly in the assessment of differences that might be found between the PR and the two sets of parameterization in terms of vertical rain structure. This limited ambition is due to the difference in the definition of rain in the observation and the model and in the possible quantitative bias that exists in the PR data due to sampling.

A short presentation of the TRMM PR specifications and data characteristics will be given to help understand the specificities of satellite rain observations. The sampling method is an important issue for this work. To characterize the main climatological structures, long time series are necessary. Three datasets are built to characterize the most relevant one for our study. Description of the LMDZ and main characteristics of the two parameterizations schemes of the convection are given. These two descriptions are critical to analyze the results presented afterward and frame the comparison. Although the representation of rain and evaporation in the lower atmospheric layers in the model are quite different from the observation, which in turns is not unbiased, this comparison gives a good insight on the possible strength and weaknesses of each parameterization.

2. Data and methods

a. TRMM data and analysis methods

In this study, we use the TRMM PR data (June–September) from 1998 to 2006. A detailed description of TRMM PR characteristics can be found in Kummerow et al. (1998). Nevertheless, an important aspect of TRMM PR that must be emphasized here is its sampling. With a swath of about 230 km, the PR visits the same location only once or twice a day and at approximately the same local time every 47.5 days (Negri et al. 2002), except at the equator where the sampling is about once every other day. Hence, one full day of PR orbit is not enough to cover the tropical belt without gaps and also a single orbit cannot completely sample large systems. Since regional distribution of rainfall in West Africa is characterized by an important variability, it is necessary to build long-range statistics of precipitation systems in West Africa. In the present study, 9 yr (1998–2006) of PR 2A25 data are used to retrieve average rain rate profiles from version 6 products. These rain rates are obtained after correction of attenuation on the measured reflectivity profiles (Meneghini et al. 2000; Iguchi et al. 2000) and using a dynamically adjusted Z–R relationship (Iguchi et al. 2000). Because our purpose is to compare observations and models and their respective definition of convective and stratiform rainfall differ, we consider only the total rainfall. All orbits passing over West Africa during the considered period are kept. To match the model spatial resolution, the statistics are built by averaging the PR data in a $1° \times 1°$ grid.

Although many attempts were made to assess the quality of the PR rain profiles, it is difficult to get a definite answer since these statistics are the only one of their kind. One can nevertheless state that two main sources of uncertainties should be kept in mind when performing the comparison with the model-based profiles. First, the attenuation correction although assumed to be quite robust (Seto and Iguchi 2007) can always be questioned locally especially over land because of soil moisture effects. This should nevertheless not affect the surface rain estimates by more than 1%–2% on average. Second, the minimum sensitivity of the PR (about 15–17 dBZ) does not necessarily give a good sensitivity to the ice phase aloft specially the content of the smaller ice particles.

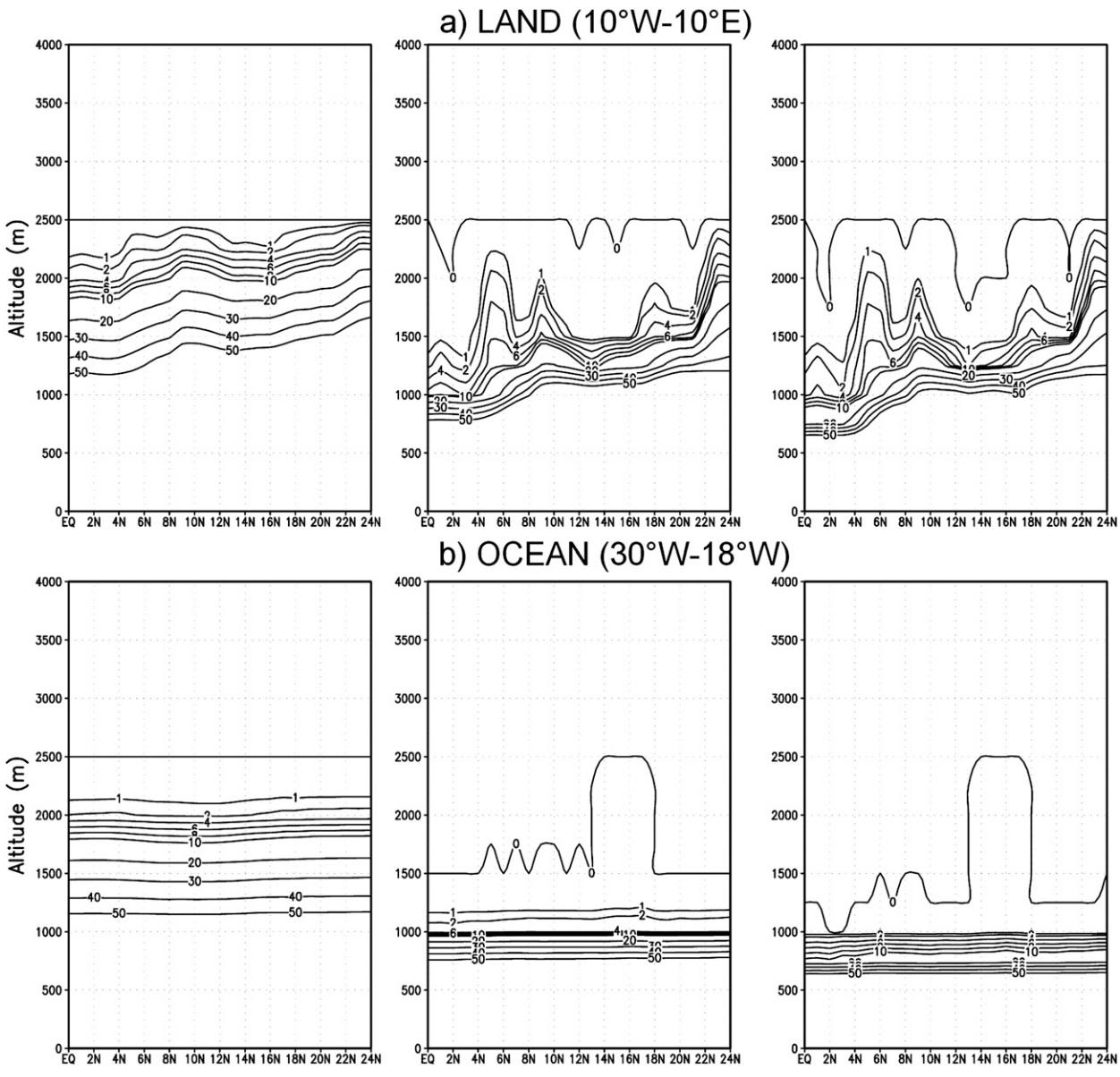

FIG. 1. Zonal percentage of lost pixels from 4 km to the ground at latitudes with the three datasets: (right) only central pixel sampling, (middle) 10-pixel sampling, and (left) full dataset: (a) over land and (b) over the ocean.

Because of the specific downward looking geometry of PR, ground clutter echoes are affecting the edges of the swath. This shadow zone affects the radar bins up to almost 2 km at the very edge of the swath, leading to a strong dependence of the number of averaged point as a function of altitude between the surface and 2-km altitude. Additionally, topography can increase this effect and some of the lower bins might then be affected by ground clutter leading to biased averages. To minimize this effect, three datasets based on different sampling strategies were tested: the first one is the full dataset [i.e., it is made of all the pixels for each PR scan (49 pixels) in order to sample the largest possible number of systems]; the second is the ''10-pixel sampling'' dataset, made with the 10 central pixels of each scan; the third dataset is the ''central pixel sampling,'' which is elaborated with the unique central pixel of each scan. The interest of this third dataset is to be able to go down as low as possible before being contaminated by ground clutters and with minimal main lobe contamination. Figure 1 shows a meridional cross section of the averaged percentage of discarded pixels with respect to the number of pixels at 4 km, on land (Fig. 1a) and on ocean (Fig. 1b) for the 3 datasets. These transects (Figs 1a,b) are used by many

authors for studying the West African monsoon features and also by models intercomparison projects like AMIP and ALMIP.

The so-called lost pixels are the pixels eliminated after quality control (i.e., eliminated pixels by 2A25 algorithm filtering). As expected, the dataset made only of the central pixel goes closer to the ground than the other datasets. Over land the 10% contour of lost pixel is just below 1.5-km altitude between latitude 0° and 22°N, and just below 2 km between latitude 22° and 24°N. Around 1.5 km, less than 4% of the pixels are lost in the equatorial region while less than 1% are lost in Sahel and between 1% and 4% are lost in Sahara. The percentages are quite similar with the 10-pixel sampling dataset (small differences are found in Sahara and Sahel), but a substantial difference can be found when compared to the full dataset. With the latter, the 10% contour of lost pixels is located around 2-km altitude and 30% at 1.5 km highlighting the ground surface echo contamination expected on the edges of the swath. Over ocean, most profiles remain valid down to 1-km altitude. The 10-pixel sampling exhibits a similar pattern, but all contours are slightly higher in altitude. When keeping all the pixels, the 10% contour of lost pixel is at around 1.75-km altitude. Since we are interested by reevaporation in the lowest atmospheric layers, we will keep only the 10-pixel sampling hereafter for the comparison, because it offers a good trade-off between the sampling and the contamination by ground clutter.

Figures 2a,b illustrate the zonal average of the vertical precipitation profiles. The average rain intensities are generally weaker over land than over ocean, but the rain signature goes higher in altitude (up to 7.5 km for land, only 5 km for ocean) and are more widely spread in latitude (from 0° to 18°N for land, only from 2° to 14°N for the ocean). Although, this unexpected heavier rain over ocean could be a problem in 2A25 v6, it is also possibly due to the comparatively small oceanic domain that was selected and that encompasses one of the region with the heaviest rain observed in western Africa: west of the Fouta-Djallon. Figure 3 shows a zonal average of the gradient of vertical retrieved rainfall rate from 4km to ground for each of the three datasets and for both oceanic and continental regions. Once again, only the levels with less than 10% of lost pixels are kept. One can notice areas with either downward decreasing (negative values) and/or downward increasing (positive values) rainfall. The Guinean gulf (0°–5°N) and the Guinean regions (5°–8°N) are generally characterized by a downward increasing rainfall while Sahel (8°–18°N) and Sahara (18°–24°N) present a downward decreasing rainfall. This decrease in rain amount as one goes closer to the ground is likely to be the combination of both reevaporation in the stratiform regions and water accumulation in convective cells. The oceanic regions are characterized in every case by a downward increasing rain probably due to a very moist air ascent coupled with shallower precipitation.

b. Model and experiment design

The time integration for the LMDZ model is done using a leapfrog scheme, with a periodic predictor–corrector time step. The monthly sea surface temperature and sea ice boundary conditions constructed at the Program for Climate Model Diagnosis and Intercomparison (PCMDI; Taylor et al. 2000) are first interpolated on the LMDZ grid and then to daily values using cubic splines (Hourdin et al. 2006). For the applications presented here, a uniform resolution of 3.75° in longitude and 2.5° in latitude with 40 levels vertical resolution is used, the time step is 3 min. Rain is calculated as combination of the precipitation from the large-scale condensation and rain condensate from convection at each pressure level. The rainfall profiles are obtained from averaging. In this study, the moist convection is parameterized by two schemes of parameterization: the Tiedtke (1989, hereafter Tiedtke's scheme), used in previous versions of LMDZ and Emanuel (1991, 1993, hereafter Emanuel's scheme), which was shown to improve significantly the large-scale distribution of tropical precipitation and in turn the simulation of the mean climate and its variability in both atmospheric (Hourdin et al. 2006) and coupled ocean–atmosphere simulations (Braconnot et al. 2007). These schemes are based on a ''mass flux'' representation of the convection updrafts and downdrafts as well as of the induced motions in the environmental air.

In Tiedtke's scheme, one convection cloud consists of a single saturated updraft. Entrainment and detrainment between the cloud and the environment can take place at any level between of the free convection level and the zero-buoyancy level. There is also one single downdraft extending from the free sinking level to the cloud base. The mass flux at the top of the downdraft is a constant fraction of the convective mass flux at the cloud base. This downdraft is assumed to be saturated and is kept at saturation by evaporating precipitation. The version used here is close to the original formulation of Tiedtke's scheme and relies on a closure in moisture convergence. Triggering is a function of the buoyancy of lifted parcels at the first grid level above condensation level.

In Emanuel's scheme, the foundations of the convective systems are regions of adiabatic ascent originating from some low-level layer and ending at their level of neutral buoyancy (LNB). Shedding from these adiabatic ascents yields, at each level, a set of drafts, which are

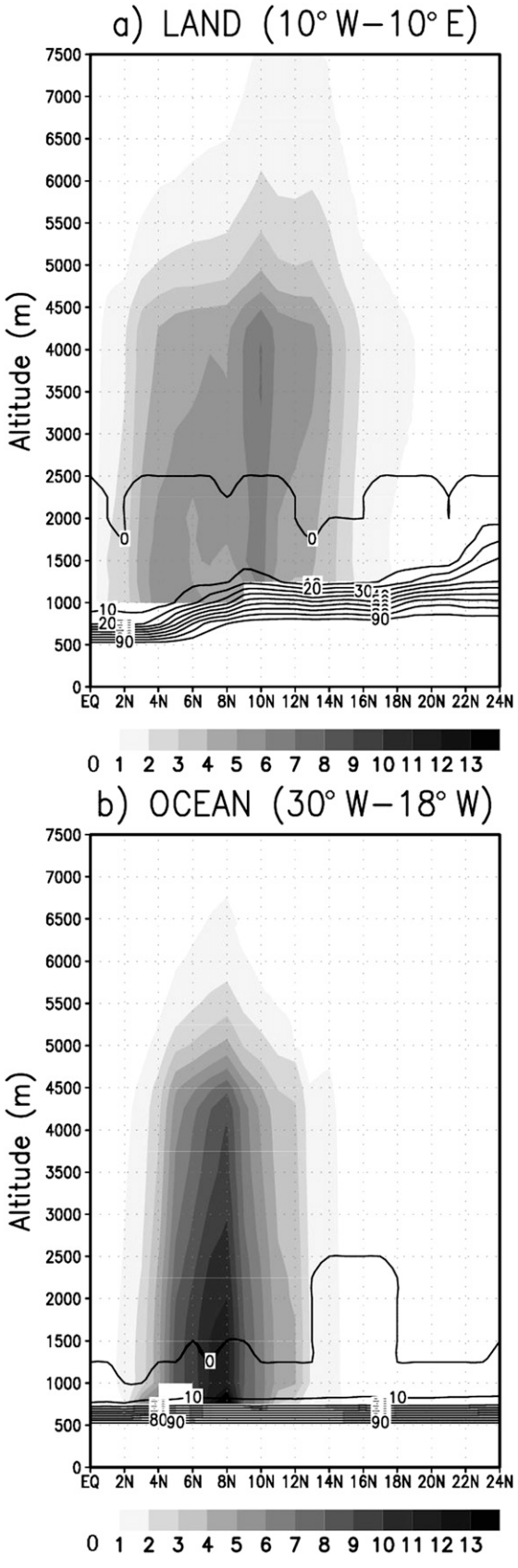

mixtures of adiabatic ascent air (from which some precipitation is removed) and environmental air. These mixed drafts move adiabatically up or down to levels where, after further removal of precipitation and evaporation of cloud water, they are at rest at their new levels of neutral buoyancy. In addition to those buoyancy-sorted saturated drafts, unsaturated downdrafts are parameterized as a single entraining plume of constant fractional area (here 1% of the grid cell) driven by the evaporation of precipitation. The version of Emanuel's scheme used here is close to Emanuel (1993). Closure and triggering take into account both tropospheric instability and convective inhibition.

Emanuel's and Tiedtke's mass flux schemes thus differ by several fundamental aspects. The triggering depends on atmospheric stability in both schemes (the max in the closure formula for Emanuel's scheme), but the closure does so only in Emanuel's scheme. Also the ratio of the downdraft to updraft mass fluxes is limited for Tiedtke's scheme (0.3 at the downdraft top), but not for Emanuel's scheme (it can be occasionally greater than 1). Those differences were shown to produce significant differences for the simulated climate (Hourdin et al. 2006).

3. Results

a. Comparison of vertical rainfall profiles

First, Fig. 4 shows the average vertical profiles classified by regions typical of the different climate systems of West Africa. Following Geerts and Dejene (2005), we interpret the vertical variation of the rain rate along a profile as the signature of some dynamic, thermodynamic, and microphysics processes occurring to the water mass during its fall from 7.5 km to the lowest available measure near the ground. Namely, these processes are in a large part the rain production in the convection and the evaporation that occurs below the freezing level in the stratiform regions. The drop size distribution evolution along the profile is taken into account by the dynamic adjustment of the *Z–R* relationship (Iguchi et al. 2000).

The observed average vertical rainfall profile in the continental Guinean regions (5°–10°N, 10°W–10°E) corresponds mostly to equatorial forests (Fig. 4a) and shows an almost constant value from the freezing level to the

←

FIG. 2. Average zonal vertical precipitation (mm h^{-1}) contours obtained from PR (threshold 10% of lost pixels) from 4 km to the ground using only central pixel sampling: over (a) land and (b) ocean. Solid lines indicate percentage of lost pixels from 4 km to ground as in Fig. 1.

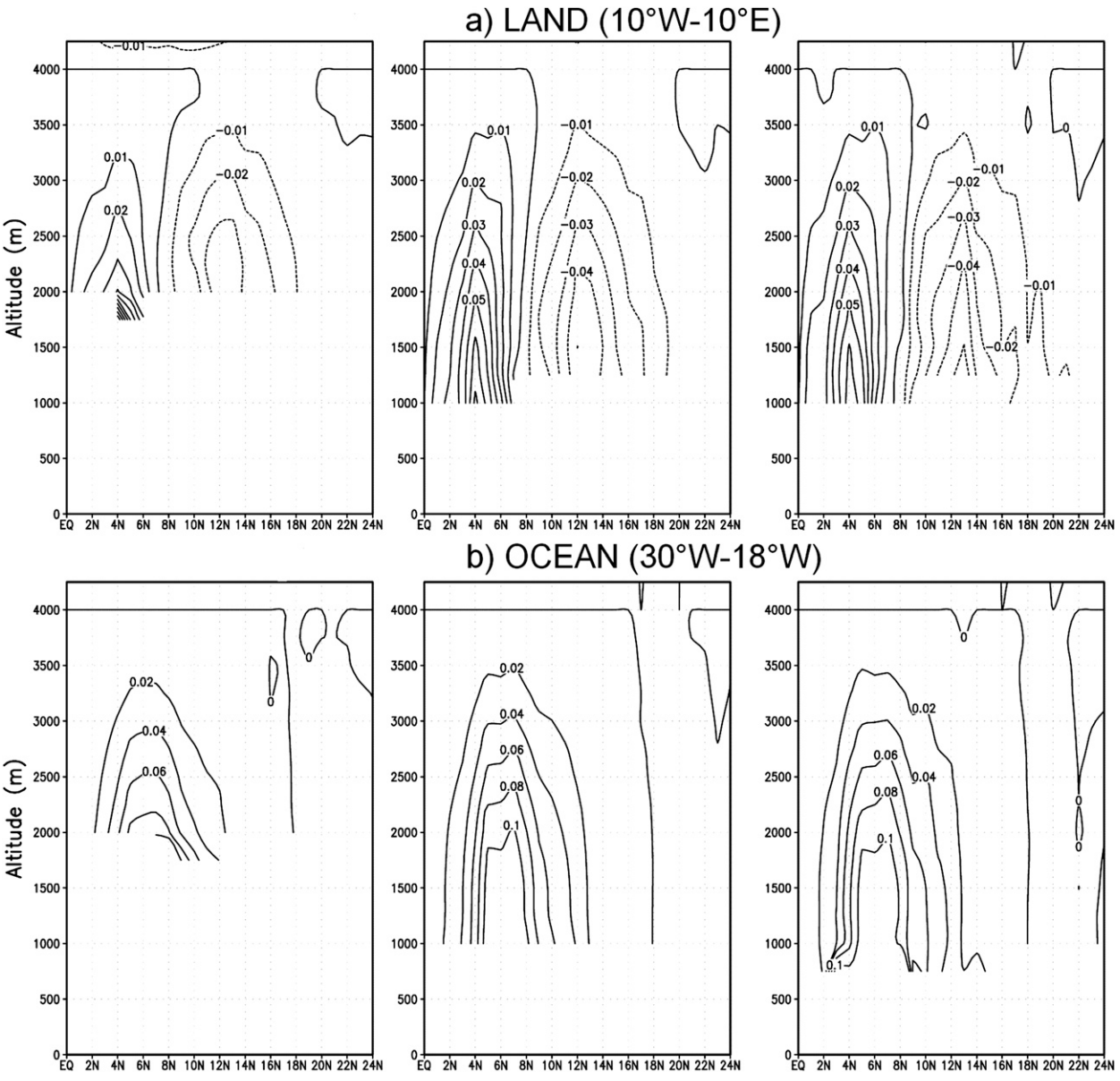

FIG. 3. As in Fig. 1, but for the zonal average of the vertical gradient of the rainfall rate (mm h^{-1} km^{-1}) from 4 km to the ground. Dashed contours indicate regions of the downward decreasing rain rate and solid contours indicate regions of the downward increasing rain rate.

ground. This is somewhat expected in this region where convection is not very intense and relative humidity is extremely high in the low levels. A rather weak updraft will produce precipitation very early during the ascent and evaporation is almost nonexistent. Above the supposed freezing level (approximately 4.5 km) the amount of precipitation decreases rapidly because of the shallow character of convection, which does not transport large amounts of supercooled water or ice phase aloft. It is possible that this decrease is amplified in the observed profiles by the comparatively lower sensitivity of the radar to the ice and specially the small ice particles. The black square at the surface in Fig. 4 shows the average surface rain over the same area obtained from the Climate Prediction Center (CPC) Merged Analysis of Precipitation (CMAP) data. The mere averaging of the PR rain rate cannot be fundamentally compared to CMAP estimates, but it provides a reference in terms of rain intensities. So, the CMAP data is assumed to be a qualitative and indirect validation of rainfall statistics built with the TRMM PR. Emanuel's scheme profile is not too far from observation below 4.5 km, but show a different

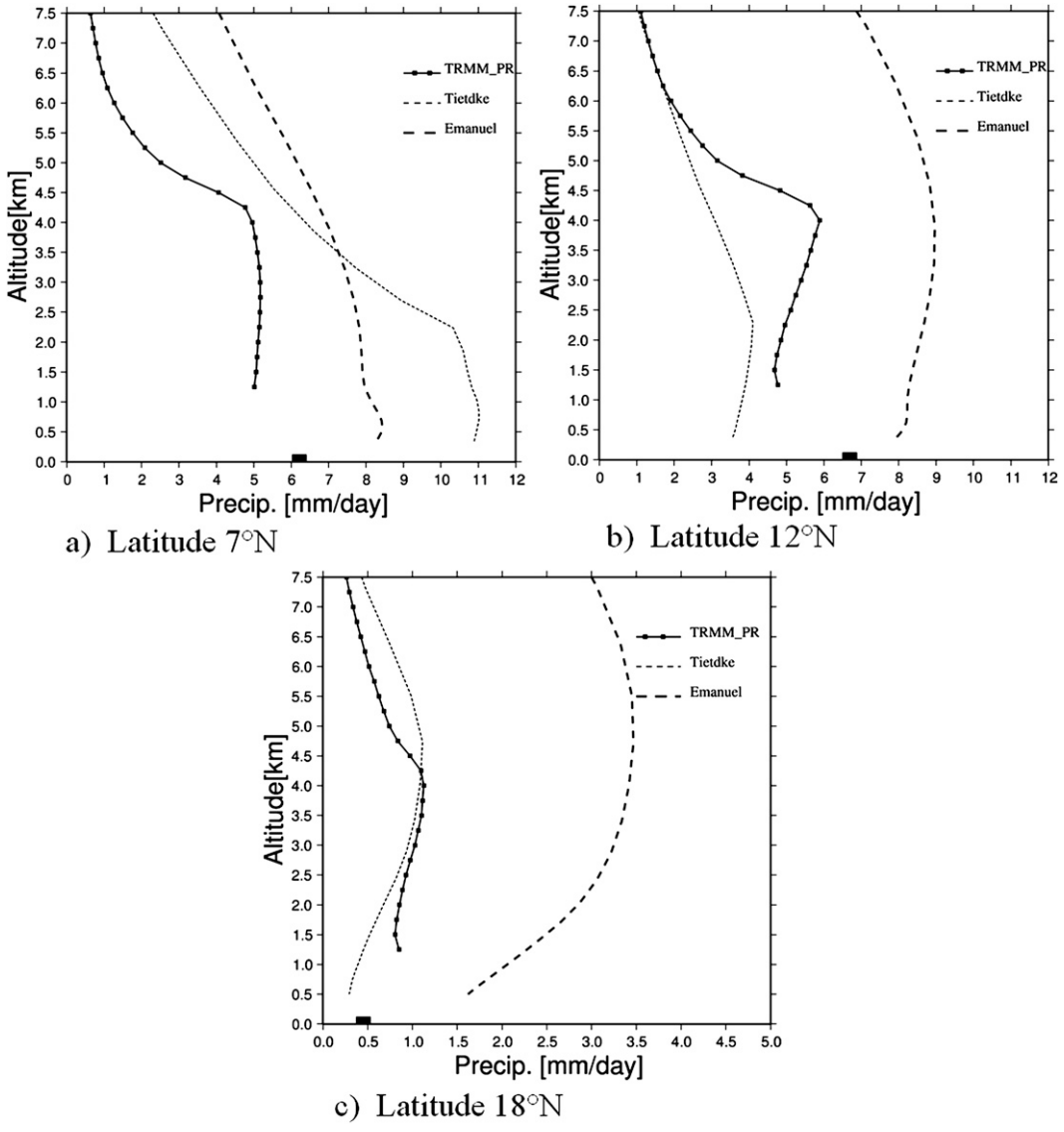

FIG. 4. Mean vertical rain profiles over land (10°W–10°E) obtained by TRMM PR and LMDZ output. TRMM PR in solid lines and LMDZ output: Emanuel's scheme (bold dashed line) and Tiedtke's scheme (dashed line). The black squares at 0-km altitude indicate precipitation at the surface obtained with CMAP data.

concavity above. Below the freezing level, the vertical gradients are close to TRMM's, but with a slightly more marked downward increase. Tiedtke's scheme exhibits a rather different behavior, the location of the main features and their intensities are quite different, although it is closer to observation in shape. This is particularly noticeable at the sharp transition at 2.25 km that occurs in the observation near the freezing level. Once again, the downward increase is slightly more pronounced below the transition region above the transition, the profile decreases rapidly with increasing altitude in a fashion that is close to the observation. The three profiles offer very different intensities at most altitudes.

In the semiarid Sahelian region 10°–17°N, 10°W–10°E (Fig. 4b), the situation is quite different. The TRMM PR rainfall profile decreases downward consistently from the brightband position (4.25 km) to 1.25 km. In our opinion, this is due to the combined effect of both the evaporation that reduces the water content as one gets closer to the ground in the stratiform regions of the cloud but also to the condensation–accumulation level that is near 4 km in the more convective regions. One must notice that the latter has a stronger effect on the profile shape (vertical gradient of rain rate) than the evaporation itself. The rain intensity above the freezing level remains high when compared to the previous case, which is the

likely signature of more intense convection. Although not having the same intensity, the TRMM PR profile and Tiedtke's scheme profiles show some similarities in terms of shape both in their upper and lower parts. Their intensity is also closer than in the previous case and the transition region position on Tiedtke's scheme profile is somewhat higher than in the previous case. Between 5.75 and 7.5 km, the Tiedtke scheme and PR profiles are merged. Below 5.5 km, Tiedtke's scheme profile is always below the observation in terms of intensities. The general features of the Emanuel's scheme profile are not so different but for the freezing level, which is not well defined: it seems to stretch between 4.75 and 3.5 km. On the other hand, below 4 km the downward decrease is well characterized with a rate similar to both observations and Tiedtke's scheme. The rainfall rate at all levels of the Emanuel's scheme profile is higher than in PR and Tiedtke's scheme profiles. The comparison with CMAP data suggests qualitatively that the TRMM PR underestimates rainfall at the surface in the Sahelian region.

Under Saharan latitude (Fig. 4c) the situation is again different. The observation does not show a very marked freezing region. From the TRMM PR observation, it seems that the Saharan rain is not very intense in average, which is the signature of a rather weak convection. This leads to a weaker water accumulation near the freezing level while evaporation might eventually remain strong. This situation is induced by the African monsoon flow that drives a precipitation gradient between the Sahara and the Sahel. The Sahel region is characterized by rains mainly due to strong and well-organized convective systems. The freezing level on both Tiedtke's and Emanuel's scheme profiles is not very well characterized either, but it seems to be in a higher position than in the observations from PR. Both profiles follow the same variation as the TRMM PR profile with a downward decrease from 4 km although it is slightly stronger in Emanuel's scheme. Tiedtke's scheme profile is close to PR profile in terms of intensities, while Emanuel's scheme is always stronger. Tiedtke's scheme reproduces the best decrease with altitude in the upper levels, but this decrease seems to start at a lower altitude.

It should be noticed that the observation show rather different features for the three different regions with a consistent evolution along the south–north transect. The two parameterizations show a somewhat similar series of changes from the Guinean coast to the Sahara.

b. Comparison of the vertical gradient seen by observations and model schemes

This part deals mostly with the low levels (below 4 km) in terms of reevaporation and liquid water production. Following Hirose and Nakamura (2002, 2004), the index of vertical gradient (IVG) was computed to quantify the vertical gradient of the rainfall rate. These authors computed their index between 2 and 3.5 km. Similarly, the IVG is defined as the first derivative of the rainfall rate between altitude H1 and H2, but the results from section 2 on rainfall profiles comparison compelled us to choose 2.25 and 1.5 km as reference altitudes (Fig. 6). IVG is expressed in millimeters per day per kilometer and the sign of this gradient suggests the importance of the production–evaporation processes along the profile. The PR data are first averaged on a $2° \times 2°$ grid matching the model resolution before the IVG is computed. Assuming that attenuation of reflectivity is well corrected in the 2A25 product (e.g., Bolen and Chandrasekar 2000) before the calculation of the rainfall rate, positive values of IVG correspond to evaporation processes in the stratiform rains and accumulation of raindrops due to updrafts in the more convective cells. On the other hand, negative values are the signature of liquid water production in the lower levels. Figures 5 and 6 present, respectively, the map and the zonal average of IVG as obtained from observations and from LMDZ with both Tiedtke's and Emanuel's parameterization scheme. The zonal variation of IVG is studied over the continental region; we have performed a zonal mean between 5°W and 5°E. The choice of this interval is meant to minimize the influence of the relief (i.e., the influence of rain mostly driven by orography).

The IVG computed from the TRMM PR shows negative values over ocean (between 15°N and 0°) and in the Guinea regions (the coast and southwest of West Africa) where water production is expected when going from the freezing level to the ground. Strong negative IVG are also found around relief regions like Fouta Djallon (southeast of Senegal) in Cameroon Hills, in Hoggar Mountain, and in the Darfur region (southeast of Chad); it is interpreted as low-level liquid water production from shallow precipitation or systematic events with low levels of convergence in these regions. The PR shows also quite consistently positive IVG over most of the rest of the continental regions where both reevaporation and water accumulation is expected to be the strongest (Fig. 5a). The maximum of reevaporation is located in the central Sahelian region (12°–15°N) with a rate around $+0.4$ mm day^{-1} km^{-1}. The minimum is slightly below $+0.1$ mm day^{-1} km^{-1} and is detected over the Saharan region. The zonal average of IVG obtained with the TRMM PR observations illustrated in Fig. 6, shows that reevaporation processes appear over the continental areas between 7° and 24°N and liquid water production processes are dominant below 7°N.

IVG computed with Tiedtke's scheme exhibits a pattern quite close to observations. Differences are noticed

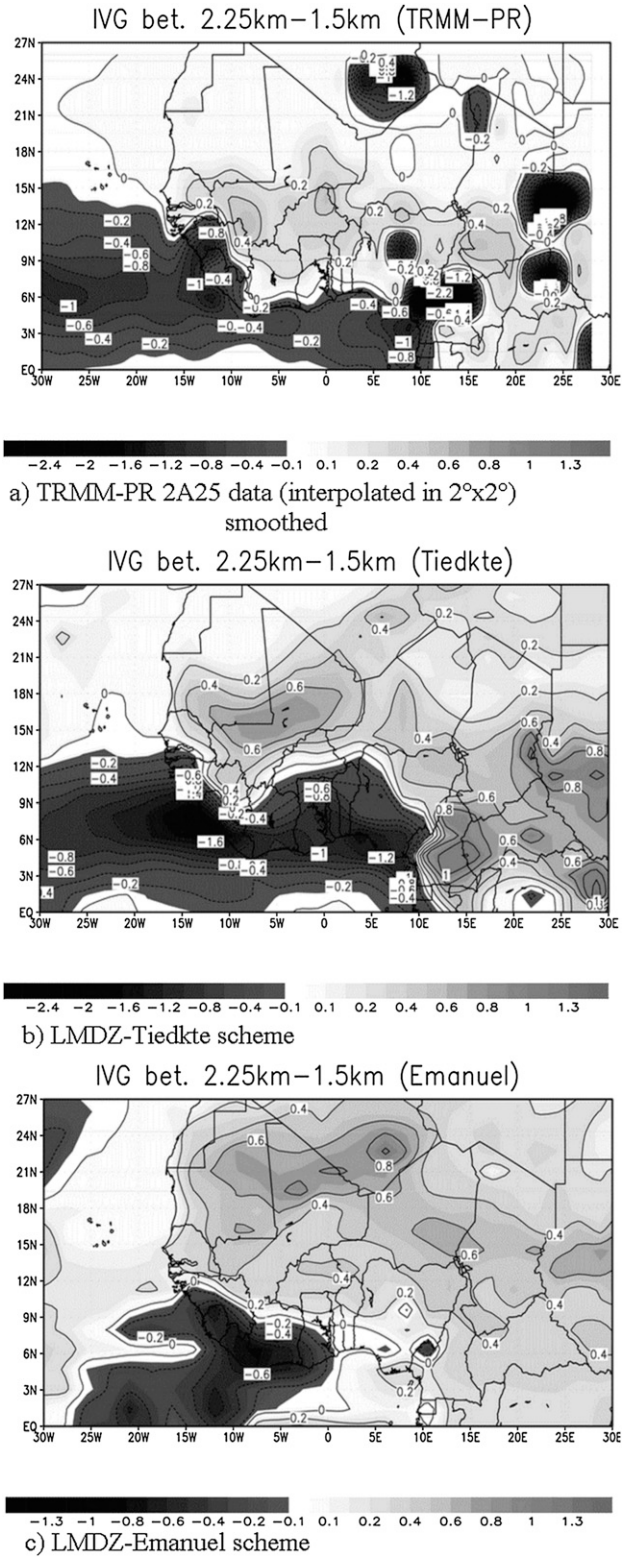

FIG. 5. Distribution of IVG computed between 2.25- and 1.5-km altitude from observations (using 10-pixel sampling) and the model: (a) TRMM PR, (b) LMDZ–Tiedkte, and (c) LMDZ–Emanuel. LMDZ output is from the climatological reference of 1981. TRMM PR is the average over JJAS from 1998 to 2006.

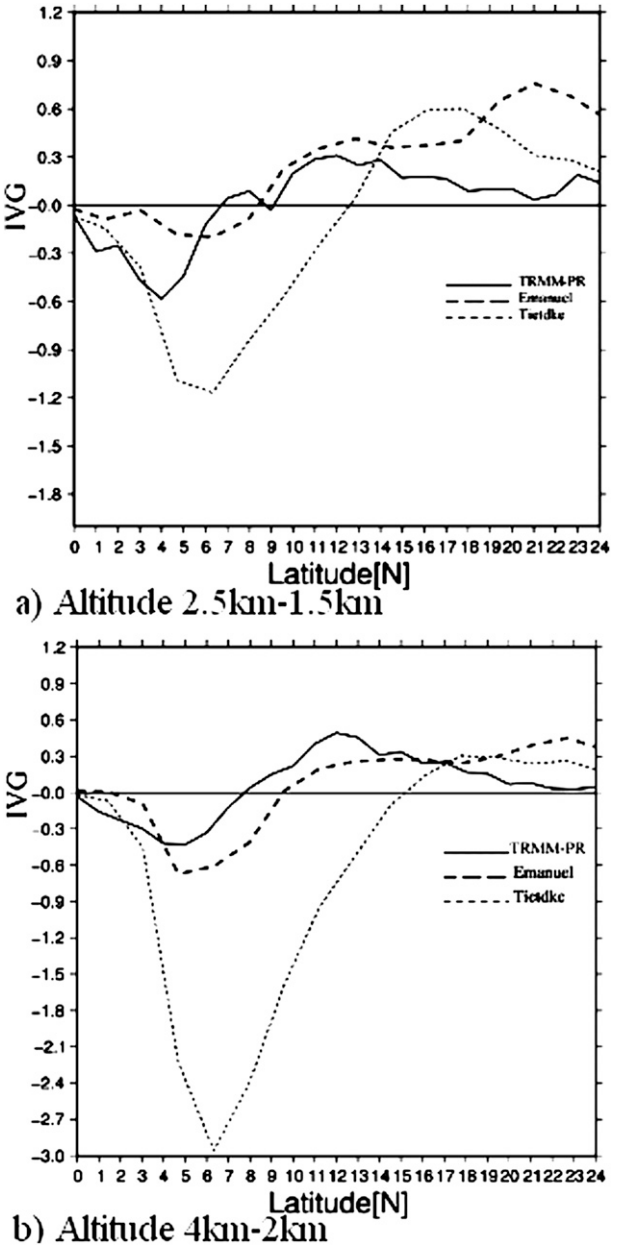

FIG. 6. Meridional IVG variation averaged between 5°W and 5°E. TRMM PR in solid line (using 10-pixel sampling dataset) and LMDZ output: altitude (a) 2.5–1.5 km and (b) 4–2 km. Emanuel's scheme (bold dashed line) and Tiedtke's scheme (short-dashed line).

with the region of negative IVG spreading too much over the continent up to 13°N. This northward extension is also clearly visible in the zonal averages (Fig. 6). In addition, positive IVG signatures are a bit too intense and extend too far (up to 20°N) when compared to observation (Fig. 5b). The maxima of IVG are observed around 16°N in Mali and around the Darfur plateau. With Emanuel's scheme, negative IVG are observed over most

of the continent and somewhat over ocean in the southwest corner of the domain. The magnitude of the IVG is very well represented in the Sahel (9°–18°N; Fig. 5c), but notably overestimated in the Sahara. This overestimate is likely associated with a much too high production of precipitation in the middle troposphere (as shown in Fig. 4c). The regional spots of negative IVG seen by the TRMM PR in the Gulf of Guinea, in the east Atlantic Ocean, and around mountain regions are well depicted by Emanuel's scheme. However, a small patch of continental negative IVG is observed over the western side of the Guinean regions and the southwestern side of the domain over ocean (between 26° and 10°W).

Analyzing Fig. 6, it appears that both Emanuel's and Tiedtke's schemes follow the observation over the landmasses. Differences can be seen for instance with the northward shift of the IVG = 0 mm day^{-1} km^{-1} in Tiedtke's scheme around 13°N (Fig. 6a) and 15°N (Fig. 6b). This is likely due to the strong overestimated amplitude of the minimum when compared to the observations.

On the other hand, Emanuel's scheme follows quite well the zonal variations of IVG seen by the TRMM PR observations (Fig. 6) with only a little shift of about 1.5° to the north. In the Sahel region, the amplitudes of Emanuel's scheme and the observations are practically identical with only minor differences where Emanuel's scheme depicts more evaporation than the observation (Fig. 6a). The Saharan latitudes are characterized by a higher rate of atmospheric reevaporation on Emanuel's scheme with a maximum near 21°N, which is not present in the observations. The latter show a very low evaporation rate in Sahara. Emanuel's scheme parameterization seems to depict a good meridional structure of IVG except in Sahara where it is overestimated.

Liquid water production processes as well as reevaporation processes obtained from the observations are roughly depicted by the two schemes of LMDZ models, but with local differences. Emanuel's scheme seems to be the best for representing the average meridional structure of reevaporation processes in mid-Sahelian latitudes where it follows very well the TRMM PR observations. It slightly underestimates the water production in equatorial regions, and extends the negative IVG region to 8.5°N where observations place it at most at 7°N. Evaporation in the Sahara region is overestimated by Emanuel's scheme with a maximum rate located in the upper Sahara. On these same zonal averages Tiedtke's scheme strongly overestimates all the processes when compared to the observations; it depicts liquid water production until 13°N with a strong intensity. The evaporation rate in the upper Sahel (15°–17°N) is also overestimated.

4. Summary and conclusions

The main objective of this paper was to study and compare vertical rainfall profiles during the West African monsoon computed from the TRMM PR data and from two different convection parameterization schemes in the LMDZ model: Tiedtke's and Emanuel's.

The average rain profiles obtained with the two schemes present both similarities and differences when compared to the TRMM PR profiles in both the upper and lower layers. The rainfall rate profiles (averaged between 10°E and 10°W) seen by Emanuel's scheme fails systematically to represent the upward decrease over 4 km. However, it catches the downward decrease seen in the observation from 4 km to the surface especially in the Sahel (proper depth of the layer dominated by reevaporation in stratiform regions–water accumulation in convection). As for Tiedtke's scheme, it provides a better description of the upward decrease in the upper level, whereas the decrease observed in the low levels starts too low (about 2 km in Sahel) compared to the observation.

The index of vertical gradient was computed from observation and compared to both parameterizations to assess how reevaporation associated with convection and water production processes are reproduced by the LMDZ climate model in the low levels of the atmosphere. The horizontal structure of IVG has shown the influence of the low-level processes that influence the convective activity and how the two model parameterizations translate it. Tiedtke's scheme seems to be able to reproduce the general structure of both negative (mostly over ocean) and positive (mostly over land) IVG, but with a signal that is generally too strong in amplitude and shows some local discrepancies at the ocean–land transition. Emanuel's scheme gives a much better range of intensities, but its general pattern seems further from the one given by the observations. Nevertheless, because the intensities are better represented the match is quite good. However, Emanuel's scheme tends to show a slightly too strong signal over the Sahara. When comparing the zonal averages the results are somewhat different. Liquid water production processes as well as reevaporation processes obtained with observations are roughly depicted by the two schemes of LMDZ models but with local differences. It seems that Emanuel's scheme offers a much better meridional gradient on average, both in terms of structure and intensities, than Tiedtke's scheme.

The behavior of parameterizations used here (as mentioned in Hourdin et al. 2006) is probably related by the fact than the updraft in Tiedtke's parameterization is an entraining plume. Both its vertical extension and intensity

are thus sensitive to the humidity of the free troposphere. While in Emanuel's scheme, the adiabatic updraft does not entrain air from the free troposphere so that the cloud top is always at LNB. A dry free troposphere can reduce convection by modifying the humidity of the mixed drafts, but not limit its vertical extension.

Acknowledgments. We would like to express our gratitude to the African Monsoon Multidisciplinary Analyses (AMMA) project for supporting this research. Based on a French initiative, AMMA was built by an international scientific group and is currently funded by a large number of agencies, especially from France, the United Kingdom, the United States, and Africa. It has been the beneficiary of a major financial contribution from the European Community's Sixth Framework Research Programme. The authors also want to thank Dr. Courtney Schumacher and the two anonymous reviewers whose comments significantly improved the quality of this paper.

REFERENCES

Bister, M., and K. Emanuel, 1997: The genesis of Hurricane Guillermo: TEXMEX analyses and a modeling study. *Mon. Wea. Rev.,* **125,** 2662–2682.

Bolen, S. M., and V. Chandrasekar, 2000: Quantitative cross validation of space-based and ground-based radar observations. *J. Appl. Meteor.,* **39,** 2071–2079.

Braconnot, P., F. Hourdin, S. Bony, J. L. Dufresne, J. Y. Grandpeix, and O. Marti, 2007: Impact of different convective cloud schemes on the simulation of the tropical seasonal cycle in a coupled ocean-atmosphere model. *Climate Dyn.,* **29,** 501–520.

Emanuel, K. A., 1991: A scheme for representing cumulus convection in large-scale models. *J. Atmos. Sci.,* **48,** 2313–2335.

——, 1993: *The Representation of Cumulus Convection in Numerical Models*. *Meteor. Monogr.,* No. 46, Amer. Meteor. Soc., 246 pp.

Geerts, B., and T. Dejene, 2005: Regional and diurnal variability of the vertical structure of precipitation systems in Africa based on spaceborne radar data. *J. Climate,* **18,** 893–916.

Hirose, M., and K. Nakamura, 2002: Spatial and seasonal variation of rain profiles over Asia observed by spaceborne precipitation radar. *J. Climate,* **15,** 3443–3458.

——, and ——, 2004: Spatiotemporal variation of the vertical gradient of rainfall rate observed by the TRMM Precipitation Radar. *J. Climate,* **17,** 3378–3396.

Houghton, J. T., Y. Ding, D. J. Griggs, M. Noguer, P. J. van der Linden, X. Dai, K. Maskell, and C. A. Johnson, 2001: *Climate Change 2001: The Scientific Basis*. Cambridge University Press, 881 pp.

Hourdin, F., and Coauthors, 2006: The LMDZ4 general circulation model: Climate performance and sensitivity to parametrized physics with emphasis on tropical convection. *Climate Dyn.,* **27,** 787–813.

Houze, R. A., 1981: Structures of atmospheric precipitation systems—A global survey. *Radio Sci.,* **16,** 671–689.

Iguchi, T., T. Kozu, R. Meneghini, J. Awaka, and K. Okamoto, 2000: Rain-profilling algorithm for the TRMM precipitation radar. *J. Appl. Meteor.,* **39,** 2038–2052.

Kummerow, C., W. Barnes, T. Kozu, J. Shiue, and J. Simpson, 1998: The Tropical Rainfall Measuring Mission (TRMM) sensor package. *J. Atmos. Oceanic Technol.,* **15,** 809–817.

Leary, C. A., and R. A. Houze Jr., 1979: Melting and evaporation of hydrometeors in precipitation from the anvil clouds of deep tropical convection. *J. Atmos. Sci.,* **36,** 669–679.

Lin, J. L., and Coauthors, 2006: Tropical intraseasonal variability in 14 IPCC AR4 climate models. Part I: Convective signals. *J. Climate,* **19,** 2665–2690.

Mapes, B. E., and R. A. Houze, 1993: Cloud clusters and superclusters over the oceanic warm pool. *Mon. Wea. Rev.,* **121,** 1398–1416.

Meneghini, R., T. Iguchi, T. Kozy, L. Liao, K. Okamoto, J. A. Jones, and J. Kwiatkowski, 2000: Use of the surface reference technique for path attenuation estimates from the TRMM precipitation radar. *J. Appl. Meteor.,* **39,** 2053–2070.

Negri, A. J., T. L. Bell, and L. Xu, 2002: Sampling of the diurnal cycle of precipitation using TRMM. *J. Atmos. Oceanic Technol.,* **19,** 1333–1344.

Schumacher, C., and R. Houze Jr., 2006: Stratiform precipitation production over sub-Saharan Africa and the tropical East Atlantic as observed by TRMM. *Quart. J. Roy. Meteor. Soc.,* **132,** 2235–2255.

Seto, S., and T. Iguchi, 2007: Rainfall-induced changes in actual surface backscattering cross sections and effects on rain-rate estimates by spaceborne precipitation radar. *J. Atmos. Oceanic Technol.,* **24,** 1693–1709.

Taylor, K. E., D. Williamson, and F. Zwiers, 2000: The sea surface temperature and sea-ice concentration boundary conditions for AMIP II simulations. PCMDI Rep. 60, Program for Climate Model Diagnosis and Intercomparison, Lawrence Livermore National Laboratory, 25 pp.

Tiedtke, M., 1989: A comprehensive mass flux scheme for cumulus parameterization in large-scale models. *Mon. Wea. Rev.,* **117,** 1779–1800.

Zipser, E. J., 1969: The role of organized unsaturated convective downdrafts in the structure and rapid decay of an equatorial disturbance. *J. Appl. Meteor.,* **8,** 799–814.

——, and K. Lutz, 1994: The vertical profile of radar reflectivity of convective cells: A strong indicator of storm intensity and lightning probability? *Mon. Wea. Rev.,* **122,** 1751–1759.